Available online at www.sciencedirect.com
SCIENCE DIRECT®
Computer Physics Communications 153 (2003) 359–372
Computer Physics Communications
www.elsevier.com/locate/cpc

A parallel monotone iterative method for the numerical solution of multi-dimensional semiconductor Poisson equation

Yiming Li [a,b]

[a] *National Nano Device Laboratories, Hsinchu 300, Taiwan*
[b] *Microelectronics and Information Systems Research Center, National Chiao Tung University, Hsinchu 300, Taiwan*

Received 9 August 2002

Abstract

Various self-consistent semiconductor device simulation approaches require the solution of Poisson equation that describes the potential distribution for a specified doping profile (or charge density). In this paper, we solve the multi-dimensional semiconductor nonlinear Poisson equation numerically with the finite volume method and the monotone iterative method on a Linux-cluster. Based on the nonlinear property of the Poisson equation, the proposed method converges monotonically for arbitrary initial guesses. Compared with the Newton's iterative method, it is easy implementing, relatively robust and fast with much less computation time, and its algorithm is inherently parallel in large-scale computing. The presented method has been successfully implemented; the developed parallel nonlinear Poisson solver tested on a variety of devices shows it has good efficiency and robustness. Benchmarks are also included to demonstrate the excellent parallel performance of the method.

PACS: 73.40.Qv; 41.20.Cv; 07.05.Tp; 02.60.Cb; 02.70.Fj

Keywords: Poisson equation; 3D semiconductor device simulation; Monotone iterative technique; Parallel computation

1. Introduction

Mathematical modeling and numerical simulation for various semiconductor devices and physics have been proven to be an indispensable alternative for the analysis and characterization of submicron or nanoscale semiconductor devices [1,5–22]. Furthermore, it provides diverse approaches in the interpretation of experimental results on material, structures, and device characteristics. The electrostatic properties for structures, binding phenomena, complex molecules, and nanoscale devices have been of great interests and studies in recent years [1–22]. Modeling and simulation for these interactions play an important role, especially in semiconductor devices and physics [1,5–22]. It is just like the molecule biophysics community requires solving a three-dimensional (3D) linear or nonlinear Poisson–Boltzmann equation for the behavior of electrostatic potential [2–4]; a multi-dimensional Poisson equation for the potential distribution should be solved numerically for semiconductor devices.

E-mail address: ymli@faculty.nctu.edu.tw, ymli@mail.nctu.edu.tw (Y. Li).

0010-4655/03/$ – see front matter
doi:10.1016/S0010-4655(03)00203-0

A set of comprehensive equations to model the classical or quantum transport phenomena, such as drift diffusion (DD), hydrodynamic (HD), Boltzmann transport, density gradient, and Schrödinger–Poisson models [1,5–22, 32–35], requires the solution of a multi-dimensional Poisson equation that describes the electrostatic potential distribution. As a result of the above models, the carriers' densities are strong nonlinear functions of the electrostatic potential that leads to the nonlinear Poisson equation [6–22]. Under different situations or iterative schemes, this nonlinear Poisson equation coupled with the above physical models can be solved separately [17–20,30,31]. Computational efficient methods for the solution of a 2D or 3D nonlinear Poisson equation are hence desired. To obtain the numerical solution of the nonlinear Poisson equation, a discretization scheme, e.g., finite difference, finite element or finite volume method [6,17,20,22–24] is firstly applied to discretize the equation. Then the discretized nonlinear Poisson equation leads to a system of nonlinear algebraic equations. The conventional methodology for the solution of this nonlinear system is based on the Newton's iterative (NI) method or its variations [6,17,20,21]. The NI method has a quadratic convergence only if the initial guess is in the neighborhood of the exact solution [17,20,21].

In this paper we propose a computational efficient solution approach, the so-called monotone iterative (MI) method [7–9,25–27], for the numerical solution of the semiconductor nonlinear Poisson equation. Based on the exponential property of the nonlinear Poisson equation, we have found the MI method converges monotonically for an arbitrary initial guess. Compared with the NI method, the MI method requires no Jacobian matrix and does not encounter any convergence problems and numerical difficulties. Furthermore, the MI algorithm is practical, easy in implementation, and inherently parallel for large-scale 3D simulation. The developed Poisson solver tested on 2D and 3D devices, such as PN diode and N-MOSFET [16] shows the efficiency and robustness. Achieved benchmarks are reported to show the parallel performance [28,29] of the method.

Subsequent sections of this paper are organized as follows. Section 2 states the semiconductor nonlinear Poisson model for an N-MOSFET at thermal equilibrium. Section 3 shows the convergence property of the MI method for the solution of the nonlinear algebraic system derived from the finite volume discretization of the nonlinear Poisson equation. Section 4 describes a parallelization scheme, the so-called domain decomposition algorithm, for the 3D parallel Poisson simulation on a Linux-cluster with message-passing interface (MPI) library. Section 5 reports the numerical results on different 2D and 3D devices; benchmark results including the achieved speedup, parallel efficiency, and load balancing are demonstrated in this section. Section 6 is the conclusions.

2. Semiconductor nonlinear Poisson model

In this section, we briefly state the formulation of the nonlinear Poisson model for a 3D MOSFET. In semiconductor devices and physics, Poisson equation is applied to describe the variation of electrostatic potential within a specified regime [16]. Consider a 3D MOSFET as shown in Fig. 1, the potential $\phi(x, y, z)$ satisfies Poisson equation in the semiconductor as follows [16–19]:

$$\frac{\partial^2\phi}{\partial x^2} + \frac{\partial^2\phi}{\partial y^2} + \frac{\partial^2\phi}{\partial z^2} = -\frac{q}{\varepsilon_s}\left(p - n + N_D^+ - N_A^-\right), \tag{1}$$

where $q = 1.60218 \times 10^{-19}C$ is the elementary charge and $\varepsilon_s = 11.9\varepsilon_0$ is silicon permittivity. The n and p are densities of free electron and hole, respectively; N_D^+ and N_A^- are the ionized donor and acceptor impurities doping concentrations, respectively (for a more general device simulation, the incomplete ionization should be considered [1,16–19]); and $\varepsilon_0 = 8.85418 \times 10^{-14}$ F/cm is the permittivity in vacuum. We now consider the Boltzmann statistics that describes the relationship between free electron density, n, and potential, ϕ, for nondegenerate semiconductors (that is the n is much smaller than the effective density of states N_C in conduction band [16]). At thermal equilibrium, this relation is given by

$$n = n_i \exp\left(q(\phi - \varphi_n)/KT\right), \tag{2}$$

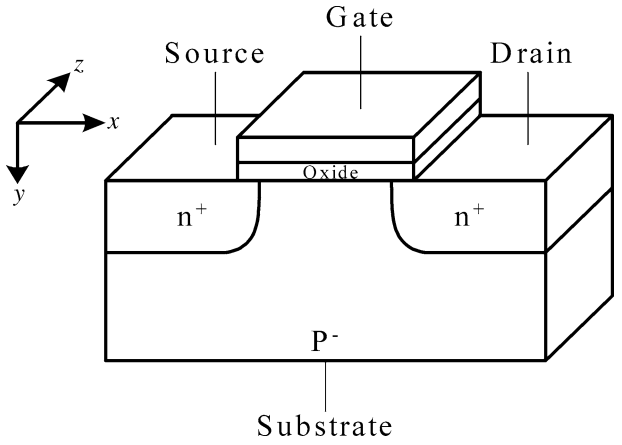

Fig. 1. A 3D schematic diagram for an N-MOSFET.

where $n_i = 9.56 \times 10^9$ cm^{-3} is the intrinsic carrier concentration, $k = 1.38066 \times 10^{-23}$ J/K is the Boltzmann constant, T is absolute temperature, and the φ_n is the imrefs or quasi-Fermi levels for electrons [16–20]. The relations for holes are similar to Eq. (2). We note that another important physics law (the so-called Fermi–Dirac statistics) has also been considered in the relationship of n and ϕ for degenerate semiconductor. Detail description of this statistics can be found [1,16]; in the Fermi–Dirac statistics, n is also a nonlinear function of ϕ which involves more complicated exponential terms. From Eqs. (1) and (2), we obtain the 3D nonlinear Poisson equation as follows:

$$\frac{\partial^2\phi}{\partial x^2} + \frac{\partial^2\phi}{\partial y^2} + \frac{\partial^2\phi}{\partial z^2} = \frac{qn_i}{\varepsilon_s}\big(u\exp(\phi/V_T) - v\exp(-\phi/V_T)\big) - \frac{q(N_D^+ - N_A^-)}{\varepsilon_s}, \tag{3}$$

where $V_T \equiv KT/q = 0.0259$ V is so-called the thermal voltage at $T = 300$ K. The u and v are defined by $\exp(-\varphi_n/V_T)$ and $\exp(\varphi_p/V_T)$, respectively. Furthermore, the nonlinear Poisson equation is supplemented by physically appropriate boundary conditions [17–20]. For device's contact terminals, source, drain, gate, and substrate, applying assumptions of the ohmic contact and charge neutrality condition [16], we have the Dirichlet type boundary condition on ϕ,

$$\phi = V_{\text{App.}} + V_T\frac{N_D^+ - N_A^-}{|N_D^+ - N_A^-|}\ln\left(\frac{N_D^+ - N_A^- + \sqrt{(N_D^+ - N_A^-)^2 + 4n_i^2}}{2n_i}\right), \tag{4}$$

where $V_{\text{App.}}$ is the applied voltage. To make the device self-contained a vanishing outward electric field, $E = -\nabla\phi$, on its boundary, the artificial boundaries on the device's surrounding environment are assumed to be a homogeneous Neumann type boundary condition

$$\frac{\partial\phi}{\partial v} = 0, \tag{5}$$

where v is the component of the outward unit normal vector on the boundary. On the interface between p^- semiconductor and oxide, by assuming the equal-flux and using the approximation that the oxide thickness, t_{ox}, is much smaller than the device channel length, we obtain the mixed type boundary condition as follows:

$$\frac{\partial\phi}{\partial v} = \frac{1}{\varepsilon_s}Q(\phi) - \frac{\varepsilon_{\text{ox}}}{t_{\text{ox}}\varepsilon_s}\phi + \frac{\varepsilon_{\text{ox}}}{t_{\text{ox}}\varepsilon_s}V_G, \tag{6}$$

where Q is the potential dependent surface interface charges, $\varepsilon_{\text{ox}} = 3.9\varepsilon_0$ is S_iO_2 permittivity, and V_G is the gate voltage. Eqs. (3)–(6) form the 3D nonlinear Poisson model problem in the semiconductor and the unknown to be

solved is the potential $\phi(x, y, z)$. When device is at thermal equilibrium without any applied voltage at contacts, the u and v are piecewise constants and equal one. The Poisson equation with $u \equiv v \equiv 1$ has to be solved to obtain the so-called equilibrium potential $\phi(x, y, z)$ [16–20].

The above 3D nonlinear Poisson model is discretized with the finite volume method over finite hexahedral volumes firstly. The corresponding system of nonlinear algebraic equations is then solved directly (without any linearization procedures) with the MI method [7–9]. This method is a kind of constructive methods for the solution of partial differential equations (PDEs) [25–27]. Based on the exponential nonlinear property on the right-hand side of the equation, we will show the MI method converges to the unique solution of the system monotonically in the next section.

3. Numerical solution with the monotone iterative method

To discretize the above PDE together with its boundary conditions in x, y, and z directions, we apply a finite volume method (FVM) with nonuniform mesh technique [17,20,22–24]. For the simplicity, we treat the problem with assumptions that $u \equiv v \equiv 1$ and $Q = 0$ [16]. Using the divergence theorem on a finite hexahedral volume and considering the tensor-product meshes for the hexahedral volume [24], the discretized Poisson equation can be written as

$$\begin{aligned}
&\xi_{i+1,j,k}\phi_{i+1,j,k} + \xi_{i-1,j,k}\phi_{i-1,j,k} + \xi_{i,j+1,k}\phi_{i,j+1,k} + \xi_{i,j-1,k}\phi_{i,j-1,k} \\
&\quad + \xi_{i,j,k+1}\phi_{i,j,k+1} + \xi_{i,j,k-1}\phi_{i,j,k-1} + \xi_{i,j,k}\phi_{i,j,k} \\
&\quad = \tau_{i,j,k}\left[\frac{qn_i}{\varepsilon_s}\left(\exp\left(\frac{\phi_{i,j,k}}{V_T}\right) - \exp\left(-\frac{\phi_{i,j,k}}{V_T}\right)\right) - \frac{q(N_D^+ - N_A^-)_{i,j,k}}{\varepsilon_s}\right],
\end{aligned} \tag{7}$$

where the arranged coefficients $\xi_{i,j,k}$ and $\tau_{i,j,k}$ for all i, j, and k are direct results from the integral approximations with the quadrature rule. After employing the boundary conditions, the above set of equations for the approximations $\phi_{i,j,k}$ at the nodes $\mathbf{X}_{i,j,k} = (x_i, y_j, z_k)$ can be written together as the compact matrix form,

$$\mathbf{A\Phi} = -\mathbf{F}(\mathbf{\Phi}), \tag{8}$$

where $\mathbf{\Phi}$ is the unknown vector formed by $\phi_{i,j,k}$ in the natural ordering, $\mathbf{F}$ is the vector of nonlinear functions corresponding to the finite volume discretization of Eqs. (3)–(6). For any vector $\mathbf{\Phi} = (\phi_n)$, the vector-valued function $\mathbf{F}$ is defined by $\mathbf{F}(\mathbf{\Phi}) = \mathbf{F}(n, \phi_n)$, $1 \leqslant n \leqslant N$, where the N is the total dimension of matrix. The function $\mathbf{F}(n, \psi)$ is bounded, i.e. there is some constant C such that $|\mathbf{F}(n, \psi)| \leqslant C$, $|\psi| \leqslant \infty$, $n = 1, 2, \ldots, N$. As a result of considering the tensor-product, the matrix $\mathbf{A}$ is a seven-banded block-tridiagonal form. We note all coefficients in Eq. (7) are nonnegative and the following relation

$$\xi_{i,j,k} \geqslant \xi_{i+1,j,k} + \xi_{i-1,j,k} + \xi_{i,j+1,k} + \xi_{i,j-1,k} + \xi_{i,j,k+1} + \xi_{i,j,k-1}$$

holds for all $\mathbf{X}_{i,j,k}$. Based on these observations, it can be shown $\mathbf{A}$ is an irreducible $\mathbf{M}$-matrix [24]. The right-hand side of Eq. (3) is continuously differentiable function with respect to ϕ, and the derivative of this nonlinear function is nonnegative. The finite volume discretization of the 3D Poisson equation with tensor-product hexahedral volume yields the matrix $\mathbf{A}$ and the following theorem can be proved.

Theorem 1. *$\mathbf{A}$ is an irreducible $\mathbf{M}$-matrix, $\mathbf{F}(n, \psi)$ is continuously differentiable, $1 \leqslant n \leqslant N$, and $\frac{d}{d\psi}\mathbf{F}(n, \psi) \geqslant 0$ for ψ is bounded, then there exists at most one solution of the nonlinear algebraic system* (8).

Proof. For any vector $\mathbf{v} = (\mathbf{v}_n)$, let $\mathbf{\Lambda}(\mathbf{v})$ be the diagonal matrix defined by

$$\mathbf{\Lambda} = \begin{pmatrix} \mathbf{F}'(1,\mathbf{v}_1) & 0 & \dots & \dots & 0 \\ 0 & \mathbf{F}'(2,\mathbf{v}_2) & 0 & \dots & \vdots \\ \vdots & \dots & \ddots & \dots & \vdots \\ \vdots & \dots & 0 & \mathbf{F}'(N-1,\mathbf{v}_{N-1}) & 0 \\ 0 & \dots & \dots & 0 & \mathbf{F}'(N,\mathbf{v}_N) \end{pmatrix},$$

where

$$\mathbf{F}'(n,\psi) \equiv \frac{d}{d\psi}\mathbf{F}(n,\psi),$$

and assume both of the $\widehat{\mathbf{\Phi}}$ and $\widetilde{\mathbf{\Phi}}$ are the distinct solutions of (8).

Let

$$\mathbf{\Phi} = \widehat{\mathbf{\Phi}} - \widetilde{\mathbf{\Phi}},$$

then

$$\big[\mathbf{A} + \mathbf{\Lambda}(\mathbf{v})\big]\mathbf{\Phi} = 0$$

for some $\mathbf{v}$. Since the matrix $\mathbf{A} + \mathbf{\Lambda}(\mathbf{v})$ is an **M**-matrix, $\mathbf{A} + \mathbf{\Lambda}(\mathbf{v})$ is a nonsingular matrix and $\mathbf{\Phi} = 0$. Thus there exists at most one solution of the nonlinear algebraic system (8). □

We now write $\mathbf{A} = \mathbf{D} - \mathbf{L} - \mathbf{U}$ and proceed to the description of the iterative method for solving the system (8) arising from the finite volume discretization of semiconductor nonlinear Poisson equation. This method for solving the multi-dimensional semiconductor nonlinear Poisson equation consists of only single iteration loop as follows:

$$(\mathbf{D} + \lambda\mathbf{I})\mathbf{\Theta}^{(m+1)} = (\mathbf{L} + \mathbf{U})\mathbf{\Theta}^{(m)} - \mathbf{F}(\mathbf{\Theta}^{(m)}) + \lambda\mathbf{I}\mathbf{\Theta}^{(m)}, \tag{9}$$

where the superscript index m is the iteration index, **D**, **L**, and **U** are diagonal, lower triangular, and upper triangular matrices of **A**, respectively. The **I** is an identity matrix and $\lambda\mathbf{I}$ is a diagonal matrix determined by the function **F**. The formula (9) can be regarded as a Jacobi type iterative scheme and is ready for parallel computing. The following theorem states the main result for this iterative method in the numerical solution of semiconductor nonlinear Poisson equation.

Theorem 2. *Assume that there is a constant* $\lambda_1 > 0$ *such that* $0 \leqslant \mathbf{F}'(n,\psi) \leqslant \lambda_1$, $|\psi| < \infty$, $n = 1, 2, \dots, N$. *Let* $\mathbf{\Theta}^{(0)} = (\theta_n^{(0)})$ *be an arbitrary vector. Let* $\mathbf{\Theta}^{(m)}$, $m \geqslant 1$, *be the solution of* (9) *with* λ_1. *Let* $\mathbf{\Phi}^* = (\phi_n^*)$ *be the solution of* (8). *Then* $\mathbf{\Theta}^{(m)} \to \mathbf{\Phi}^*$, *as* $m \to \infty$.

Proof. Let

$$\mathbf{W}^{(m)} = \mathbf{\Theta}^{(m)} - \mathbf{\Phi}^*.$$

Then from Eq. (9), we have

$$(\mathbf{D} + \lambda_1\mathbf{I})\mathbf{W}^{(m+1)} = (\mathbf{L} + \mathbf{U})\mathbf{W}^{(m)} + \lambda_1\mathbf{W}^{(m)} - \big(\mathbf{F}(\mathbf{\Theta}^{(m)}) - \mathbf{F}(\mathbf{\Phi}^*)\big). \tag{10}$$

For some η_n we have

$$\mathbf{F}\big(n,\theta_n^{(m)}\big) - \mathbf{F}\big(n,\phi_n^*\big) = \mathbf{F}'(n,\eta_n)\big(\theta_n^{(m)} - \phi_n^*\big).$$

Let $\mathbf{\Lambda}(\boldsymbol{\eta})$ be the diagonal matrix defined by

$$\mathbf{\Lambda}(\boldsymbol{\eta}) = \begin{pmatrix} \mathbf{F}'(1,\eta_1) & 0 & \dots & \dots & 0 \\ 0 & \mathbf{F}'(2,\eta_2) & 0 & \dots & \vdots \\ \vdots & \dots & \ddots & \dots & \vdots \\ \vdots & \dots & 0 & \mathbf{F}'(N-1,\eta_{N-1}) & 0 \\ 0 & \dots & \dots & 0 & \mathbf{F}'(N,\eta_N) \end{pmatrix}.$$

Then

$$(\mathbf{D}+\lambda_1\mathbf{I})\mathbf{W}^{(m+1)} = \big(\mathbf{L}+\mathbf{U}+\lambda_1\mathbf{I}-\mathbf{\Lambda}(\boldsymbol{\eta})\big)\mathbf{W}^{(m)}.$$

It is possible to choose a proper λ_1, such that

$$\big(\mathbf{L}+\mathbf{U}+\lambda_1\mathbf{I}-\mathbf{\Lambda}(\boldsymbol{\eta})\big) \geqslant 0.$$

So

$$(\mathbf{D}+\lambda_1\mathbf{I})|\mathbf{W}^{(m+1)}| \leqslant \big(\mathbf{L}+\mathbf{U}+\lambda_1\mathbf{I}-\mathbf{\Lambda}(\boldsymbol{\eta})\big)|\mathbf{W}^{(m)}|.$$

On the other hand, we note

$$\big(\mathbf{L}+\mathbf{U}+\lambda_1\mathbf{I}-\mathbf{\Lambda}(\boldsymbol{\eta})\big) \leqslant (\mathbf{L}+\mathbf{U}+\lambda_1\mathbf{I}),$$

and hence

$$(\mathbf{D}+\lambda_1\mathbf{I})|\mathbf{W}^{(m+1)}| \leqslant (\mathbf{L}+\mathbf{U}+\lambda_1\mathbf{I})|\mathbf{W}^{(m)}|.$$

Denote the ratio P as follows:

$$\mathbf{P} = (\mathbf{D}+\lambda_1\mathbf{I})^{-1}(\mathbf{L}+\mathbf{U}+\lambda_1\mathbf{I}),$$

we have

$$|W^{(m+1)}| \leqslant P^{(m+1)}|W^{(0)}|.$$

Thus

$$P^{(m)} \to 0 \quad \text{as } m \to \infty,$$

and the result is followed [24]. □

This result demonstrates the solution sequence generating from iterative formula (9) will converge to the solution of Eq. (8) for all choices of the initial guess $\mathbf{\Theta}^{(0)}$. Furthermore, the above iterative method can also apply to the solution of the Poisson equation where the Fermi–Dirac statistics and incomplete ionization are included. We can further verify that those nonlinear functions on the right-hand side of the Poisson equation are bounded functions of ϕ due to the finite input applied voltage. Therefore, we have the following corollary.

Corollary. *Assume that there is a constant $M > 0$ such that $|\mathbf{F}(n,\psi)| \leqslant M$ and a constant $k > 0$ which satisfies $|\mathbf{F}(n,\psi_1) - \mathbf{F}(n,\psi_2)| \leqslant k|\psi_1 - \psi_2|$, $|\psi| < \infty$, $|\psi_1| < \infty$, $|\psi_2| < \infty$, and $n = 1, 2, \dots, N$. Let $\mathbf{\Theta}^{(0)} = (\theta_n^{(0)})$ be a vector which satisfies $\mathbf{A}\mathbf{\Theta}^{(0)} \geqslant -\mathbf{F}(\mathbf{\Theta}^{(0)})$. Let $\mathbf{\Theta}^{(m)}$, $m \geqslant 1$, be the solution of* (9). *Let $\mathbf{\Phi}^* = (\phi_n^*)$ be a solution of* (8). *Then $\mathbf{\Theta}^{(m)} \to \mathbf{\Phi}^*$, as $m \to \infty$.*

Proof. With a similar process in Theorem 1 above, this proof can be done by direct calculation and the definition of the constant k. □

This corollary states that if the nonlinear function is bounded, then the solution sequences $\mathbf{\Theta}^{(m)}$ converge monotonically from above to a solution $\mathbf{\Phi}^*$ of Eq. (8). We note if $\overline{\Phi}$ is the maximal solution of Eq. (8) and $\mathbf{\Theta}^{(0)} \geqslant \overline{\Phi}$, then $\Phi = \overline{\Phi}$. Similarly if $\mathbf{\Theta}^{(0)}$ satisfies $\mathbf{A}\mathbf{\Theta}^{(0)} \leqslant -\mathbf{F}(\mathbf{\Theta}^{(0)})$, then $\mathbf{\Theta}^{(m)} \to \mathbf{\Phi}^*$, as $m \to \infty$. Moreover, if $\underline{\Phi}$ is the minimal solution of Eq. (8) and $\mathbf{\Theta}^{(0)} \leqslant \underline{\Phi}$, then $\Phi = \underline{\Phi}$. To clarify the MI computational procedure, we summarize the MI algorithm as follows [7].

Step M1. Take an initial guess for $\Phi^{(m)}$.
Step M2. Let $m = 1$ and set $(i, j, k) = (1, 1, 1)$.
Step M3. Determine the MI parameter λI instantaneously.
Step M4. Compute the $\Phi^{(m+1)}$ with Eq. (9).
Step M5. Perform convergence test. If it converges, then break, else $m = m + 1$ and return to M3.

Together with a decoupling algorithm (the so-called Gummel's method in semiconductor device simulation [17,18,20,30,31]), the MI method for the numerical solution of the nonlinear Poisson equation can be applied to solve various semiconductor device models. For examples, the DD model consists of three coupled nonlinear PDEs, the Poisson equation, the electron current continuity equation, and the hole current continuity equation. Transport behavior of submicron MOSFET devices is governed with these coupled PDEs and is solved with the Gummel's decoupled method sequentially; that is in the DD model the Poisson equation is solved for $\phi^{(g+1)}$ given the previous states $n^{(g)}$ and $p^{(g)}$. The electron current continuity equation is solved for $n^{(g+1)}$ given $\phi^{(g)}$ and $p^{(g)}$. The hole current continuity equation is solved for $p^{(g+1)}$ given $\phi^{(g)}$ and $n^{(g)}$, where g is the index of outer iterations. A similar procedure can be applied to decouple PDEs of the HD model. Each decoupled PDE is discretized with FVM and is solved with the MI method. Details of the numerical simulation and comparison with the measured data for N-MOSFET and DTMOSFET devices have been studied in our recent works [8,9]. For a 3D simulation, to obtain highly accurate solution, it is necessary to perform the calculation with a fine mesh. However, the increase of grid points is numerically expensive and requires huge CPU time. For this reason, we further introduce a parallelization algorithm to reduce the computational time in the next section.

4. A domain decomposition parallelization algorithm

Based on the iterative formula (9), we present the corresponding multi-dimensional parallel domain decomposition algorithm. Once the tree structure is established, according to the total number of nodes, the number of processors for computing will be assigned and allocated. Then a geometric graph partitioning method in x-, y-, and/or z-directions, as shown Fig. 2, is applied to partition the number of nodes to each processor dynamically. The arrangement of all nodes to each processor is based on a dynamic partition algorithm. Ideally, all the partitioned sub-domains should contain approximately the same number of nodes to ensure a good load balance among the processors. The computational procedure for parallel domain decomposition is outlined.

Step D1. Initialize the MPI environment and parameters.
Step D2. Based on the mesh configuration, we establish the corresponding tree structure.
Step D3. Count the number of grid points and applies the *dynamic partition algorithm* to determinate how many processors are required in this simulation.
Step D4. All assigned jobs are solved with formula (9). Computed results are communicated with the MPI protocol. For a given iteration since our iterative algorithm (9) is of the Jacobi type scheme, all points through this formula are decoupled and solved independently in each sub-domain. We note that once previous results are given, the boundaries for partitioned sub-domains are totally separated and we solve

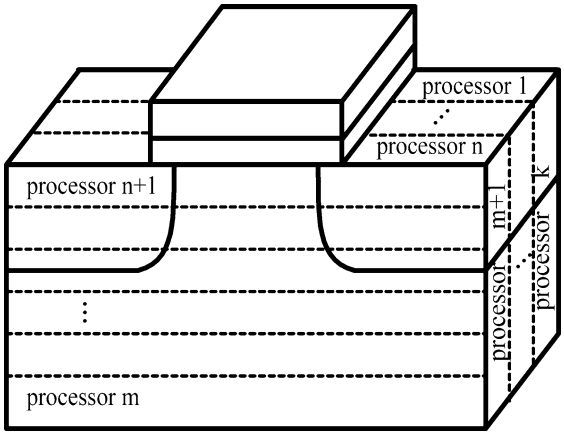

Fig. 2. A 3D partition for the parallel domain decomposition.

each nonlinear system independently. When newer MI solutions of nonlinear systems are computed, we perform the boundary data exchange of the sub-domains so that each sub-domain knows about the nodes value on neighbors for the next iteration loop.

Step D5. Perform convergence test for all cubic cells and run the mesh refinement for those cubic cells whose diagonal difference of the solution is greater than a specified tolerance error.

Step D6. Repeat D3–D5 until the error of all cubic cells is less than the specified tolerance error.

Step D7. Host processor collects all computed results and stops the MPI environment.

The load balancing *dynamic partition algorithm* applied in D3 above consists of some sub-steps.

Step P1. Count the total number of nodes.

Step P2. Estimate the optimal number of processors.

Step P3. The number of nodes will be assigned to each processor is equal to the total nodes divided by the optimal number of processors.

Step P4. Along x-, y-, and z-direction in the 3D device domain, search (from left to right, bottom to top, and front to back) and assign nodes to these processors sequentially.

Step P5. Repeat P4 until all nodes have been assigned.

We note that the searching direction may be changed in the neighborhood of p-n junctions for maintaining the best load balancing performance. The parallel algorithm can also be applied to a 2D problem. It has been implemented on a Linux-cluster with the MPI library. The constructed Linux-cluster contains 16 PCs (CPU: AMD 1 GHz, Memory: 256 Mbytes, and operation system: LINUX RedHat 7.2), the files access and share are through network file system and network information system. The user datagram protocol controlled by MPI is applied to short distance fast communication.

Fig. 3 illustrates the parallel program organization; the pre-processor performs several tasks, and one of the tasks is to manage the input data required for each parallel processor. In the Linux-cluster with the MPI configuration, input data are prepared on the host machine and sent to each client through TCP/IP with high speed switch. Tested on a 3D MOSFET, we have verified the parallel implementation has good efficiency and parallel speedup on the constructed Linux-cluster.

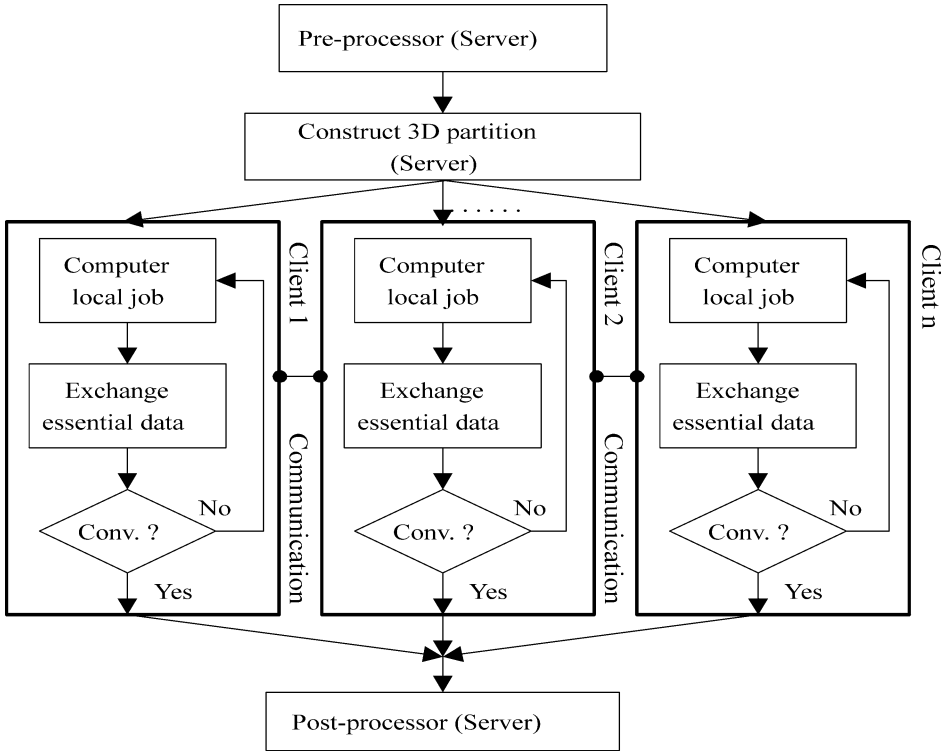

Fig. 3. An illustration of the parallel algorithm and organization.

5. Results and discussion

We now present 2D and 3D simulation results of the developed parallel 3D Poisson simulator to show the robustness and efficiency of the method. Parallel results such as speedup, efficiency, and load balancing [28,29] are also included in this section. In the numerical simulation, the MI parameter λI is computed with the newer iterative results and updated for next solution iterations instantaneously [7].

The first example is a 2D PN diode [16] under applied bias $V_A = 0.5$ V. For the 2D PN diode, as shown in the inserted figure of Fig. 4, the Poisson equation (3) is solved with the Dirichlet type boundary condition (4) on the n and p contacts. The rest parts of the boundary of the simulation domain are assumed to be the Neumann type boundary condition (5). The doping profile inside the n^+ region is 10^{17} cm^{-3} and is 10^{15} cm^{-3} for the p^- region, respectively. The simulation domain of this PN diode is defined on a 3.5×3.5 μm^2 and the n^+ region is a quarter ellipsoid with radius 0.5 μm. Fig. 4 shows the computed potential at applied voltage equals 0.5 V. The convergence criterion is the maximum potential difference between two successive iterations less than 10^{-6} V_T for all nodes. The mesh size is about 1000 nodes. As shown in Fig. 4, the simulated result indicates clearly that there is a junction jump layer on the n^+ and p^- regimes. To test the validity of the method, we simulate more complicated 2D and 3D MOSFET devices. The second example is a 0.35 μm N-MOSFET with oxide thickness 7 nm [16] on a 2D domain. The doping profile in this simulation comes from realistic device structure. Fig. 5 shows the doping profile and Fig. 6 illustrates the computed potential at thermal equilibrium condition. The convergence criterion is of the maximum error less than 10^{-8} V_T and the mesh size equals 2200 nodes. The third example concerns 3D 0.25 μm N-MOSFET simulation. The doping profile is a Gaussian distribution with 10^{20} cm^{-3} in the ellipsoid n^+ regions and 10^{17} cm^{-3} in the p^- region. The oxide thickness is 7 nm. The simulation domain is 1.1 μm in x and y directions where the z direction is 40 μm. The convergence criterion is the same with Example 2 and the mesh

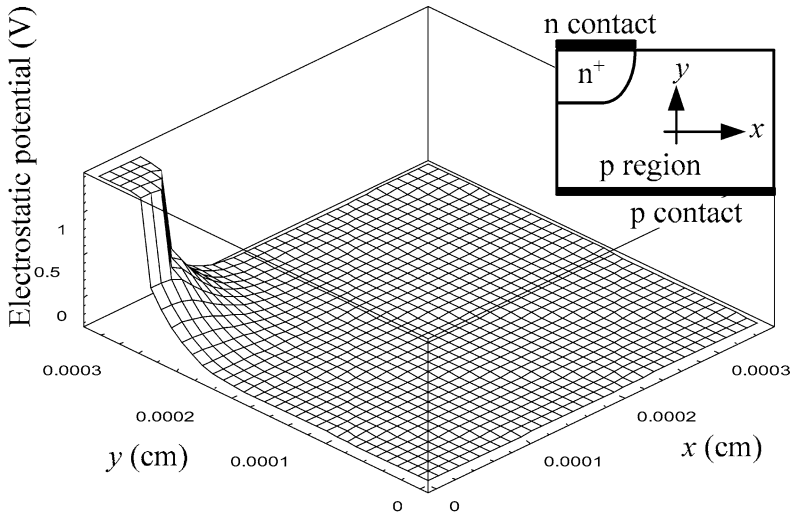

Fig. 4. The simulated potential of the 2D PN diode.

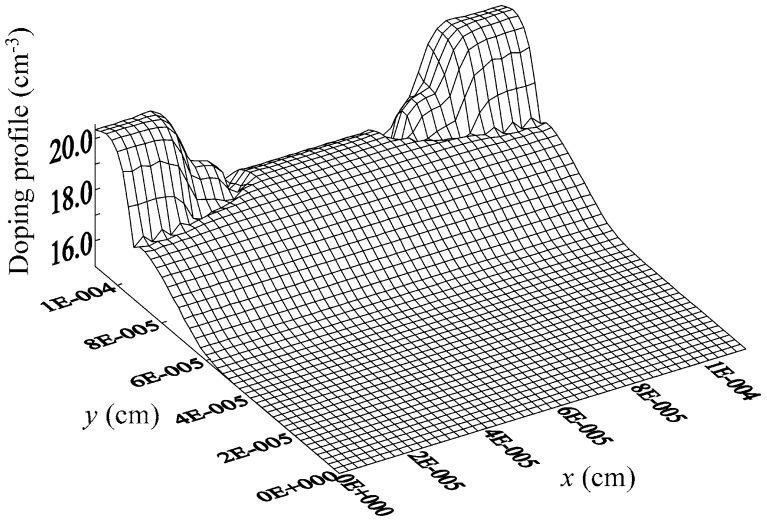

Fig. 5. A surface plot of the input doping concentration for the 0.35 μm N-MOSFET.

size is about 64000 nodes. Fig. 7 presents the calculated result for this device at $V_{GS} = V_{DS} = 2.0$ V. We further verify the global convergence property for the proposed method. The test device is the same with Example 3 but at $V_{GS} = V_{DS} = 0$ V. There are four different initial guesses tested, 0.0 V, charge neutrality condition, -5.0 V and 5.0 V. As shown in Fig. 8, the monotonic convergence behavior is confirmed. It takes only about 100 s CPU time for these different calculations on the computing system. However, for the same device structure and same test condition, the conventional NI method does not converge with the initial guesses -5.0 V and 5.0 V, respectively. For such bias the NI in general requires a more precise initial guess [32] to start the solution procedure. However, in practical device simulation it is difficult to calculate a proper initial guess for different structures and models, especially in nanoscale devices [11,33,34]. On the other hand, the MI method in solving the Schrödinger–Poisson

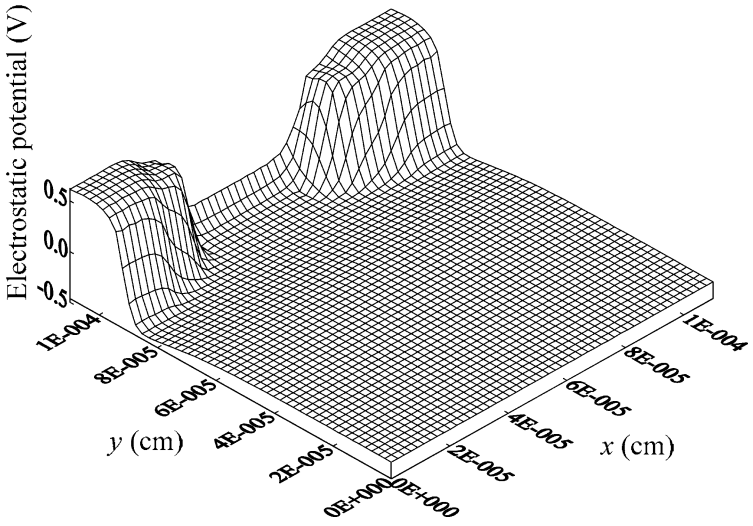

Fig. 6. The potential distribution of Example 2.

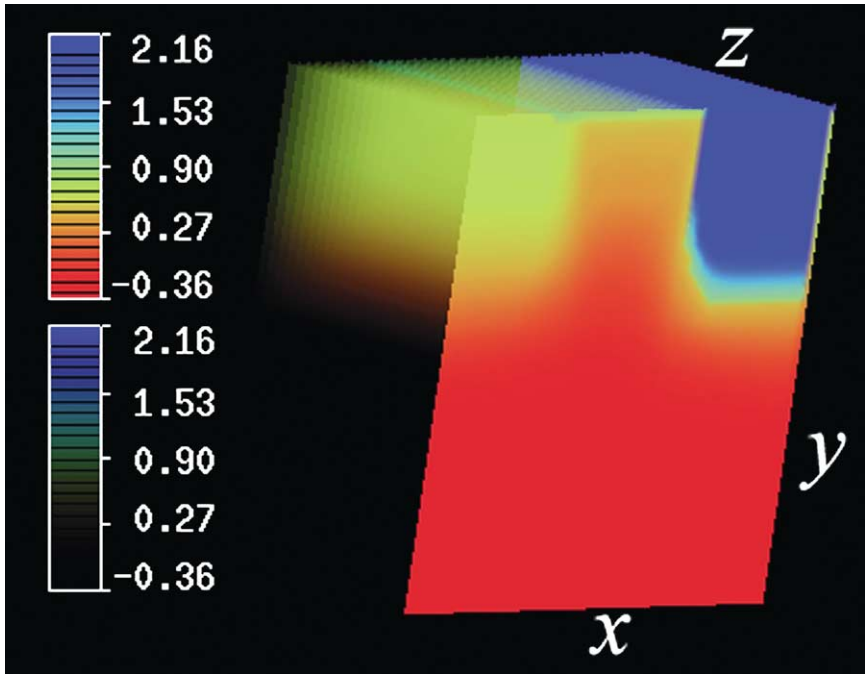

Fig. 7. The simulated potential of the 3D 0.25 μm N-MOSFET. The upper color bar is for $x-y$ plane and the other is for $y-z$ plane.

and density gradient models was implemented successfully; its robust convergence property was confirmed and the simulated results were compared with measured data in our recent works [35,36].

We report the achieved parallel performances for the 3D simulation. The speedup is the ratio of the code execution time on a single processor to that on multiple processors and the efficiency is defined as the speedup divided by the number of processors. As shown in Fig. 9 and Table 1, the parallel speedup efficiency, and load

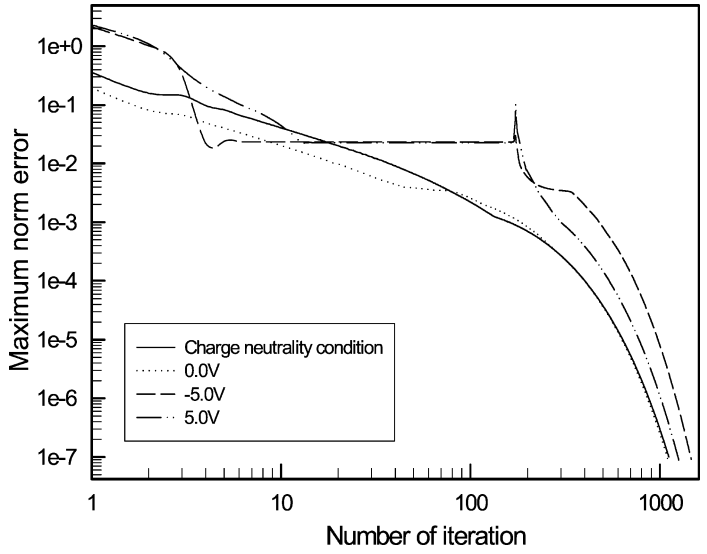

Fig. 8. The global convergence of the MI method for the 3D N-MOSFET simulation at $V_{GS} = V_{DS} = 0$ V.

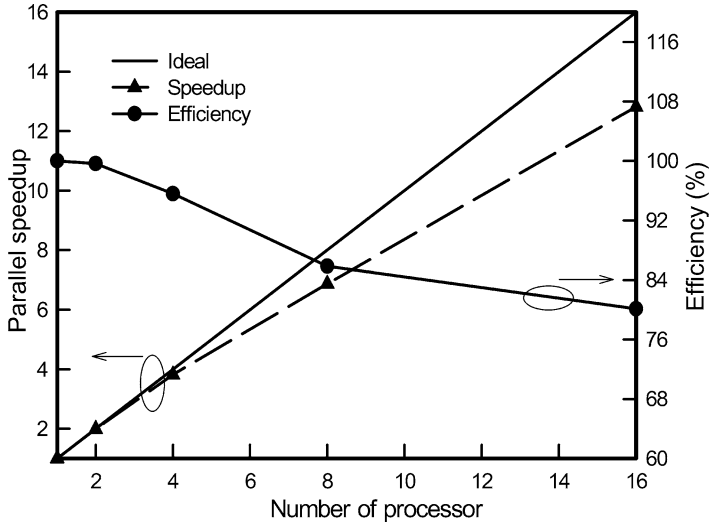

Fig. 9. The achieved speedup and efficiency of the 3D N-MOSFET simulation on the 16-CPUs Linux-cluster. The mesh consists of 512000 nodes.

balancing for a 3D N-MOSFET at $V_{GS} = V_{DS} = 1.5$ V are shown, where the test device is the same with Example 3. The maximum difference is defined as the maximum difference of the code execution time divided by the maximum execution time [28,29]. Table 1 shows the dynamic load balancing of domain decomposition for the 3D N-MOSFET simulation on the 8-processors Linux-cluster. When the number of nodes increased, the load balancing tends to a fixed value at 2%. A very good load balancing, 2.14%, for the 3D simulation with 256000 mesh size has been obtained on the 8-processors Linux-cluster with MPI library. For the 16-processors Linux-cluster, we have similar load balancing result. As shown in Fig. 9, the achieved speedup is 13.0 and the efficiency is about 80% on the 16-processors Linux-cluster.

Table 1
The achieved load balancing for the 3D N-MOSFET simulation

Nodes	Parallel time (s)								Maximum difference (%)
	CPU No.								
	#0	#1	#2	#3	#4	#5	#6	#7	
64000	18	18	18	18	18	18	18	18	0.00
100000	117	116	116	114	117	114	114	115	2.56
144000	734	730	720	734	734	719	719	734	2.04
256000	3362	3361	3362	3321	3298	3360	3290	3305	2.14

6. Conclusions

We have proposed a parallel simulation approach to the solution of multi-dimensional Poisson equation with the MI method. The MI method applied to solve 3D semiconductor nonlinear Poisson equation has been successfully implemented on a 16-processors Linux-cluster with MPI library. Mathematically we proved that this solution technique has a global convergence property. Numerical results confirmed the MI method is superior to conventional NI methods in the solution of semiconductor Poisson equation. Achieved speedup, efficiency and load balancing have been presented to show the computational performance. We conclude that this solution algorithm can be utilized to solve various semiconductor device and physics models. Furthermore, with a similar investigation on the nonlinear property of the PDE, this method provides an efficient alternative in the solution of the Poisson equation that derived from different biological, physical, chemical, and engineering problems.

Acknowledgements

The author expresses his appreciation to the referee for an exceptional in-depth reading of the manuscript. This work was supported in part by the National Science Council (NSC) of Taiwan, under contract numbers NSC 91-2112-M-317-001, NSC 91-2815-C-317-001-E, NSC 91-2215-E-321-001, PSOC 91-EC-17-A-07-S1-0011, and by the grants from the 2002 Research Fellowship Award of the Pan Wen-Yuan Foundation in Taiwan.

References

[1] S.M. Sze, Semiconductor Devices, Physics and Technology, Wiley, New York, 2002.
[2] B. Honig, A. Nicholls, Science 268 (1995) 1144–1149.
[3] A. Neumaier, SIAM Rev. 39 (1997) 407–460.
[4] M.J. Kim, B.J. Yoon, J. Colloid Interface Sci. 236 (2001) 173–179.
[5] R.W. Dutton, A.J. Strojwas, IEEE Trans. Computer-Aided Design Integr. Circuits Systems 19 (2000) 1544–1560.
[6] A. Asenov, et al., Simul. Practice Theory 4 (1996) 155–168.
[7] Y. Li, et al., in: Proceedings of Technical Papers of 1999 International Symposium of VLSI Technology, Systems, and Applications, 1999, pp. 27–30.
[8] Y. Li, et al., Engrg. Comput. 18 (2002) 124–137.
[9] Y. Li, et al., Comput. Phys. Comm. 147 (2002) 697–701.
[10] J.W. Jerome, SIAM J. Appl. Math. 45 (1985) 565–590.
[11] A. Pacelli, IEEE Trans. Electron Devices 44 (1997) 1169–1171.
[12] P. Degond, et al., SIAM J. Sci. Comput. 22 (2000) 986–1007.
[13] A. Wettstein, et al., IEEE Trans. Electron Devices 48 (2002) 279–284.
[14] Y. Omura, et al., Solid-State Electron. 44 (2000) 1511–1514.
[15] O. Simonetti, et al., J. Non-Crystalline Solids 280 (2001) 110–115.
[16] S.M. Sze, Physics of Semiconductor Devices, 2nd edn., Wiley-Interscience, New York, 1981.
[17] S. Selberherr, Analysis and Simulation of Semiconductor Devices, Springer-Verlag, New York, 1984.

[18] P.A. Markowich, et al., Semiconductor Equations, Springer, Vienna, 1990.
[19] J.S. Yuan, J.J. Liou, Semiconductor Device Physics and Simulation, Plenum Press, London, 1998.
[20] R. Bank, et al., IEEE Trans. Electron Devices ED-30 (1983) 1031–1041.
[21] A. Trellakis, U. Ravaioli, Comput. Methods Appl. Mechanics Engrg. 181 (2000) 437–449.
[22] S. Sacco, F. Saleri, Numer. Methods Partial Differential Equations 13 (1997) 215–236.
[23] P.I. Crumpton, et al., J. Comput. Phys. 109 (1993) 1–15.
[24] R.S. Varga, Matrix Iterative Analysis, Springer, New York, 2000.
[25] S. Heikkilä, V. Lakshmikantham, Monotone Iterative Techniques for Discontinuous Nonlinear Differential Equations, Marcel Dekker, New York, 1994.
[26] Y. Deng, et al., Math. Comp. 65 (1996) 943–982.
[27] J. Wang, Nonlinear Anal. 35 (1998) 113–142.
[28] P.S. Pacheco, Parallel Programming with MPI, Morgan Kaufmann, San Francisco, CA, 1997.
[29] K. Dowd, C. Severance, High Performance Computing, O'Reilly, Sebastopol, 1998.
[30] D.L. Scharfetter, H.K. Gummel, IEEE Trans. Electron Devices 16 (1969) 66–77.
[31] H.K. Gummel, IEEE Trans. Electron Devices 11 (1964) 455–465.
[32] T.Y. Wong, et al., in: Proceedings of the 1995 IEEE International Conference on Microelectronics and VLSI, 1995, pp. 218–221.
[33] F. Stern, J. Comput. Phys. 6 (1970) 56–67.
[34] T. Kerkhoven, et al., J. Appl. Phys. 68 (1990) 3461–3469.
[35] Y. Li, et al., Comput. Phys. Comm. 147 (2002) 214–217.
[36] Y. Li, WSEAS Trans. Circuit 1 (2002) 1–6.